

# **Study of a dissipative particle dynamics based approach for modeling suspensions**

by

**Nicos S. Martys  
Building and Fire Research Laboratory  
National Institute of Standards and Technology  
Gaithersburg, MD 20899 USA**

**Reprinted from Journal of Rheology, Vol. 49, No. 2, pp. 401-424, March-April 2005.**

**NOTE: This paper is a contribution of the National Institute of Standards and Technology and is not subject to copyright.**

**NIST**

**National Institute of Standards and Technology**  
Technology Administration, U.S. Department of Commerce

# Study of a dissipative particle dynamics based approach for modeling suspensions

Nicos S. Martys<sup>a)</sup>

*Materials and Structures Division, Building and Fire Research Laboratory,  
National Institute of Standards and Technology, Gaithersburg, Maryland 20899*

(Received 2 June 2004; final revision received 9 November 2004)

## Synopsis

In this paper, a dissipative particle dynamics (DPD) based approach for modeling suspensions is examined. A series of tests is applied comparing simulation results to well established theoretical predictions. The model recovers the dilute limit intrinsic viscosity prediction of Einstein and provides reasonable estimates of the Huggins coefficient for semidilute suspensions. At higher volume fractions, it was necessary to explicitly include lubrication forces into the algorithm as the usual DPD interactions are too weak to prevent overlaps of the rigid bodies and account for other related effects due to lubrication forces. Results were then compared with previous studies of dense hard sphere suspensions using the Stokesian dynamics method and experimental data. Comparison of relative viscosity values determined from strain controlled shearing versus stress controlled shearing simulations are also given. The flow of spheroidal objects is studied. The rotation of a single spheroid under shear is consistent with the predictions of Jeffery. Simulations of sheared spheroids at higher volume fractions produce an apparent nematic phase. An example is given of the application of DPD to model flow in another geometry, gravitational driven flow between parallel cylinders, which is of practical interest. © 2005 The Society of Rheology, Inc.. [DOI: 10.1122/1.1849187]

## I. INTRODUCTION

The flow properties of suspensions (e.g., colloids, ceramic slurries, and concrete) are of fundamental interest and play an important role in a wide variety of technological processes crucial to industry [Larson (1999)]. There have been many theoretical advances in understanding the rheological properties of simple suspensions (e.g., very dilute and semidilute suspensions, suspensions composed of spheroidal objects), however, understanding the flow of more complex suspensions (e.g., dense suspensions, random shaped particles, suspensions composed of particles that interact) remains a great challenge. Here, computational modeling can play an important role in investigating the properties of such systems. One possible approach is to apply standard computational fluid dynamics methods. This involves considerable effort in carrying out the difficult task of tracking boundaries between different fluid and solid phases, usually involving various meshing, moving grid, and interpolation schemes to account for motion of the rigid bodies. A second approach, based on the lattice Boltzmann method [Ladd (1997); Nguyen and Ladd (2002)], involves calculation of the momentum transfer which results from particles

---

<sup>a)</sup>Electronic mail: nicos.martys@nist.gov

that “bounce” off the rigid body. The kinetics of the momentum transfer has to be carefully evaluated as the rigid body’s surface can be located at any point and with any orientation between the lattice nodes from which the particles “propagate.” A third, and perhaps best known approach, is called Stokesian dynamics (SD) [Brady and Bossis (1988); Phung and Brady (1996); Sierou and Brady (2001)]. In many respects, Stokesian dynamics serves as a standard benchmark as it was the first computational method to properly incorporate long range hydrodynamic interactions, Brownian forces, and lubrication forces for modeling suspensions composed of hard spheres. Some of its successes include the demonstration of shear induced ordering and shear thickening in dense hard sphere systems [Foss and Brady (2000)]. Recently, a new computational method, called dissipative particle dynamics (DPD) [Hoogerbrugge and Koelman (1992); Koelman and Hoogerbrugge (1993)] has shown promise for modeling a variety of complex fluid systems. Further, DPD may potentially have some advantages over some computational fluids dynamics based approaches in that DPD can naturally accommodate many boundary conditions while not requiring meshing (or remeshing) of the computational domain. On the surface, DPD looks very much like a molecular dynamics algorithm where, in that case, particles subject to interatomic forces move according to Newton’s laws. However, the particles in DPD are not atomistic but, more so, a mesoscopic representation of the fluid.

One can take several “philosophical” views of DPD. Ideally, one would like to think of DPD as a consequence of the systematic coarse graining of atomistic or microscopic domains. Indeed, there has been much effort in this direction [Flekkøy *et al.* (2000)]. While this view provides a general framework for understanding the structure of the DPD equations, there are still several gaps in bridging the microscopic and macroscopic domains. For example, it is necessary to impose constitutive relations (e.g., stress-strain rate relations) at some point. Hence, further work is needed to make such scale-up procedures clearer. A second view is that DPD belongs to a class of Lagrangian formulations of the Navier–Stokes equations {e.g., smooth particle hydrodynamics [Monaghan (1992)]}. Related but more sophisticated models [Serrano and Español (2001); Español (1998)] utilize Voronoi cells to establish a grid that fills space or associate a time dependent volume parameter [Español and Serrano (1999)] to each DPD particle. From this perspective, DPD does not conserve volume in a proper sense, making the implementation of arbitrary equations of state difficult [Español and Serrano (1999); Español and Revenga (2003)]. In this respect, one can think of DPD as a “poor man’s” Lagrangian formulation of the Navier–Stokes equations having sacrificed some rigor for computational expediency. For a third view, and what was probably the original intent, one can think of DPD as a somewhat abstract cellular-automata-based construct that, in certain regimes, recover hydrodynamics consistent with the Navier–Stokes equations {similar, in a way to how lattice gas and lattice Boltzmann methods were originally thought of [Rothman and Zaleski (1994)]}. Indeed, it has been shown, by mapping the DPD equations to an equivalent stochastic differential equation (the Fokker Planck equation) [Español and Warren (1995)] and applying a Chapman–Enskog analysis [Marsh *et al.* (1996, 1997)], DPD does produce hydrodynamic behavior consistent with the Navier–Stokes equations to second order in the Chapman–Enskog expansion. Thus, the challenge is to carefully connect solutions obtained from DPD to physical regimes of interest {cf. [Groot and Warren (1997); Dzwinel and Yuen (2000, 2002)]}. Hopefully, universal features of both the cellular automata approach and the “real” physical system can be exploited to help gain insight into the system of interest. Regardless of what computational approach or philosophical view one takes, it is extremely important to validate the computational method, especially if it is going to be used as a predictive computational tool.

Previous papers [Koelman and Hoogerbrugge (1993); Boek *et al.* (1997)] have demonstrated the potential of DPD to model colloidal suspensions including hard sphere and spheroidal objects [Boek *et al.* (1997)]. However, comparisons with experiments and theory have been more qualitative rather than quantitative and there were no comparisons with other approaches. In this paper, a DPD based approach for modeling suspensions is examined with an emphasis on comparing simulation results to well known theoretical predictions concerning simple flow scenarios and the rheology of dilute to semidilute suspensions. Tests include comparisons with the intrinsic viscosity prediction of Einstein and the Huggins coefficient for dilute and semidilute suspensions, respectively. At higher volume fractions, the DPD algorithm had to be modified to include lubrication forces as the usual DPD interactions are too weak to prevent overlap of the rigid bodies. Results are compared with previous studies concerning the flow of dense suspensions based on the Stokesian dynamics method and experimental data. As an alternative to the commonly used Lees–Edwards boundary condition [Allen and Tildesley (1987)], which can, roughly be thought of as a constant applied strain rate, simulations were also carried out using a constant applied stress. It was found that use of a constant stress to drive the system helped mitigate large temporal fluctuations in the derived viscosity which occurred in the constant strain rate case. Interestingly, rheological measurements at higher volume fractions are often carried out using a constant applied stress. Spheroidal rigid bodies are also considered. The rotation period of a single prolate spheroid under shear is consistent the predictions of Jeffery (1922); Eirich (1967). Studies of the flow of spheroids at higher volume fractions produce an apparent nematic phase [Larson (1999)]. An example of application of the DPD algorithm to model flow in other geometries like that encountered in the flow and placement of concrete is given. To contrast this work with previous DPD based simulations of suspensions [Boek *et al.* (1997)], it should be noted that in this paper lubrication forces are explicitly included in the simulations of dense sphere suspensions. In addition, size polydispersivity, Jeffery’s orbits and the onset of an apparent nematic phase were studied. Finally, flow in alternate geometries and under applied stress instead of applied strain were examined.

## II. BASIC DPD EQUATIONS

I start by briefly reviewing the basic equations of DPD. In DPD, as in molecular dynamics, the evolution of the position,  $\mathbf{r}_i$ , and momentum,  $\mathbf{p}_i = m \mathbf{v}_i$ , of particle  $i$  with mass,  $m$ , and velocity  $\mathbf{v}$  are described by

$$\dot{\mathbf{r}}_i = \mathbf{v}_i, \quad (1)$$

$$\dot{\mathbf{p}}_i = \sum_{j \neq i}^N \mathbf{F}_{ij}, \quad (2)$$

where  $\mathbf{F}_{ij}$  is the force on particle  $i$  due to particle  $j$  and the dot indicates a time derivative. Interparticle forces are typically represented as three types: conservative  $\mathbf{F}_{ij}^C$ , dissipative  $\mathbf{F}_{ij}^D$ , and random  $\mathbf{F}_{ij}^R$  so that

$$\mathbf{F}_{ij} = \mathbf{F}_{ij}^C + \mathbf{F}_{ij}^D + \mathbf{F}_{ij}^R. \quad (3)$$

The conservative force is simply a central force, derivable from some effective potential  $\phi_{ij}$ . The dissipative force is proportional to the difference of velocity,  $\mathbf{v}_{ij} = \mathbf{v}_i - \mathbf{v}_j$ , between particles and acts to slow down their relative motion, producing a viscous effect. The random force (usually based on a Gaussian random noise) helps maintain the temperature of the system and provides an additional viscous effect. The three forces are given below

$$\mathbf{F}_{ij}^C = - \frac{\partial \phi_{ij}}{\partial \mathbf{r}_i}, \quad (4)$$

$$\mathbf{F}_{ij}^D = - \gamma \mathbf{w}_D(\mathbf{r}_{ij}) [\hat{\mathbf{e}}_{ij} \cdot \mathbf{v}_{ij}] \hat{\mathbf{e}}_{ij}, \quad (5)$$

$$\mathbf{F}_{ij}^R = \sigma \mathbf{w}_R(\mathbf{r}_{ij}) \hat{\mathbf{e}}_{ij} \chi_{ij}. \quad (6)$$

The distance between the DPD particles  $i$  and  $j$  is given by  $r_{ij}$ ,  $\hat{\mathbf{e}}_{ij}$  is a unit vector pointing from particle  $j$  to particle  $i$ ,  $w_R(r_{ij})$  and  $w_D(r_{ij})$  are weight functions and  $\chi_{ij}$  is a randomly fluctuating variable described by Gaussian statistics. It can be shown that, in order to maintain a well defined temperature by way of consistency with the fluctuation-dissipation theorem [Español and Warren (1995)], coefficients describing the strength of the dissipative ( $\gamma$ ) and random ( $\sigma$ ) forces must be coupled, that is

$$k_b T = \frac{\sigma^2}{2\gamma}, \quad (7)$$

where  $k_b$  is the Boltzmann constant and  $T$  is the temperature. Further, so that the DPD fluid system possess a Gibbs–Boltzmann equilibrium state, the following relation must hold (detailed balance for an infinitesimal time step) [Español and Warren (1995)]:

$$w_D = w_R^2. \quad (8)$$

In this study, the choice of parameters and weight functions closely follow that described in Groot and Warren (1997). Here,  $w_R(r_{ij}) = 1 - r_{ij}$  for  $(r_{ij} < 1)$  and  $w_R(r_{ij}) = 0$  for  $r_{ij} \geq 1$ . All lengths described in this paper are defined in units of the cutoff radius,  $r_c = 1$ , of the DPD interaction. The conservative force is taken to be  $\mathbf{F}_{ij}^C = F_m(1 - r_{ij})\hat{\mathbf{e}}_{ij}$ . For all the simulations in this paper,  $\sigma \geq 40$  and  $F_m = 75k_b T / \rho$  where  $\rho$  is the global density of DPD particles. Units of  $k_b T$  are chosen such that  $k_b T = 1$  and  $F_m$  was chosen so that the DPD fluid has the same compressibility of water [see the discussion in Groot and Warren (1997)].

An important parameter that characterizes suspensions under shear is the Peclet number, Pe. Peclet number is a dimensionless number describing the competition between viscous and Brownian forces and, for spheres, is given by  $\text{Pe} = 6\pi\mu a^3 \dot{\gamma} / k_b T$ . Here,  $\mu$  is the viscosity,  $a$  is the sphere radius, and  $\dot{\gamma}$  is the shear rate. Also, for spheres under shear, the Reynolds number is given by  $\text{Re} = \rho a^2 \dot{\gamma} / \mu$ . In general  $\text{Re} \approx O(1)$  or smaller in this study. Depending on the simulation, system sizes were  $15^3$ ,  $45^3$ , and  $90^3$  in our units. Finally, because the DPD interactions are short range the code parallelized in a fairly efficient manner. For example, a spatial decomposition version of our code scaled nearly linearly up to about 16 processors on a Linux cluster. For more information on the parallelization of this code see Sims and Martys (2004).

## A. Integration of the equations of motion

The original DPD algorithm [Koelman and Hoogerbrugge (1993); Boek *et al.* (1997)] used a simple Euler algorithm for time integration. It has been noted, in Groot and Warren (1997), that use of a modified velocity-Verlet algorithm leads to improvements in numerical accuracy as well as a better characterization of thermal equilibrium properties for the DPD simulation [for a discussion of various integration schemes see Vattulainen *et al.* (2002)]. The original velocity Verlet algorithm [Verlet (1967)] is widely used in simulations and is an example of a second order symplectic integrator that has minimal computational memory requirements. It has the form

$$x(\delta t) = x(0) + v(0)\delta t + \frac{(\delta t^2)}{2}a(0), \quad (9)$$

$$v(\delta t) = v(0) + \frac{\delta t}{2}[a(0) + a(\delta t)], \quad (10)$$

where  $a(0) = F[x(0)]/m$  is the acceleration term evaluated using  $x(0)$  and an intermediate velocity  $\tilde{v}(0)$ . The velocity Verlet algorithm does not provide a prescription for including velocity dependent forces as found in DPD. To extend the velocity Verlet algorithm to include velocity dependent forces we follow Groot and Warren (1997), where  $a(0) = F[x(0), \tilde{v}(0)]/m$  and define  $\tilde{v}$  to be

$$\tilde{v}(\delta t) = v(0) + \frac{1}{2}\delta ta(0). \quad (11)$$

To model rigid body motion in a fluid, a subset of the DPD particles are initially assigned a location in space such that they approximate the shape of the object. The motion of these particles is then constrained such that their relative positions never change. The total force and torque are determined from the DPD interparticle interactions and the rigid body moves according to the Euler equations for rigid bodies. The Euler equations were solved using a quaternion based computational approach proposed by Omelyan (1998). The details of this algorithm and its adoption for DPD are given in Martys and Mountain (1999).

## B. Initialization

Groot and Warren (1997) found that choosing a number density of three DPD particles per unit volume (where as defined earlier, the unit of length is  $r_c$ ) was a practical choice for modeling the fluid phase. The equilibrium properties of the fluid are reasonably well defined here and going to higher densities quickly becomes expensive computationally. The rigid bodies were introduced by randomly placing their center of mass positions in the simulation cell. This sphere packing process, of course, leads to overlaps of the rigid bodies. A repulsive force was introduced that pushed the overlapping rigid bodies apart. Once the spheres were separated, the final configuration was used as an input for beginning the simulations.

For most of the results presented, a Lees–Edwards boundary condition [Allen and Tildesley (1987)] was used. It effectively produces a shearing effect akin to an applied constant strain rate at the boundaries. Applications of other boundary conditions will be described later in the paper.

## C. Determination of kinematic viscosity

The stress tensor has contributions from the propagation of momentum and interparticle forces

$$\sigma_{\alpha\beta} = \frac{1}{Vm} \sum_i \tilde{p}'_{i\alpha} \tilde{p}'_{i\beta} + \frac{1}{2V} \sum_{ij} F_{ij}^\alpha (r_i - r_j)_\beta, \quad (12)$$

where  $i, j$  refers to different particles,  $\alpha$  and  $\beta$  refer to Cartesian coordinate axes and  $\tilde{\mathbf{p}}'_i$  is the momentum of particle  $i$  relative to the macroscopic velocity field midway between its trajectory during a time step. Then, for a constant applied shear rate, the kinematic viscosity  $\nu$  is obtained from

$$\nu = -\sigma_{12}/\dot{\gamma}, \quad (13)$$

where the shear is applied in the  $x_1$  direction.

#### D. Accounting for constraint forces

The velocity Verlet algorithm is broken up into two parts where one alternates between updating the positions and velocities of particles. As pointed out by Koelman and Hoogerbrugge (1993), there is an additional contribution to the stress tensor due to the constraint forces that maintain the relative positions of particles the rigid body are composed of. Clearly, we are using an algorithm that does not explicitly determine the constraint forces on each particle of the rigid body. However, since we know the position and velocity of each particle, we can effectively backout the constraint forces by mapping the individual particle's (contained on the rigid body) trajectory to the velocity Verlet algorithm and then solve for the constraint forces that would be required for such motion of the particles to take place. Note that the constraint forces used to update the position and then the velocities are not the same. The difference is actually small and ignoring either contribution alone results in an error of order  $\delta t^3$  in the stress tensor (which should be symmetric up to that order). Although this agreement seems reasonable, a symmetric stress tensor is required to demonstrate that angular momentum is conserved. By incorporating the contributions of the constraint forces from the two steps of the velocity Verlet algorithm, it was found that the stress tensor was symmetric up to the order of precision of the computer (i.e., 16 figures for double precision).

We also compared our approach to determining the stress tensor to an entirely different but commonly used method described in Allen and Tildesley (1987). Here the constraint forces are not used to determine the stress tensor. Instead, the center of mass force each rigid body has on the other is utilized [cf. Allen and Tildesley (1987)]. This approach has the undesirable feature that it does not produce a symmetric tensor for short times but when averaged over long times approaches the correct symmetry. It was found that the time average stress tensor determined by both approaches were reasonably close in value and that they asymptotically approached each other over time.

### III. COUETTE AND POISEUILLE FLOW

As a first test of the code, it was examined whether simple Couette and Poiseuille flow could be recovered. Figure 1 shows a spatially and temporally averaged flow field for the system undergoing Couette flow where the Lees–Edwards boundary condition is being imposed. The spatial averaging was done over a cubic array of bins with length 1 on a side. Due to the stochastic term in the DPD equations the instantaneous flow field will appear noisy, hence, the flow field was averaged over 100 separate time steps. The fluid viscosity was determined from the simulation by calculation of the stress tensor using Eqs. (12) and (13). Next, Poiseuille flow was obtained by dividing the simulation cell in half and applying a body force in opposite directions in each cell half. Figure 2 shows the spatially and temporally averaged velocity profile in one cell after it had relaxed to its equilibrium profile. The solid line is a fit to the analytical solution of the Stokes equation with a similarly applied body force and a no slip boundary condition imposed at the cell boundaries. The only adjustable parameter in the fit was the fluid viscosity. The viscosity obtained from fitting these data was within a percent of that obtained from direct calculation of the stress tensor for the previously described Couette flow simulation, showing that the hydrodynamics was self consistent. As a corollary, this Poiseuille flow simulation demonstrates that a noslip boundary condition can be approximated, at a fluid-wall inter-

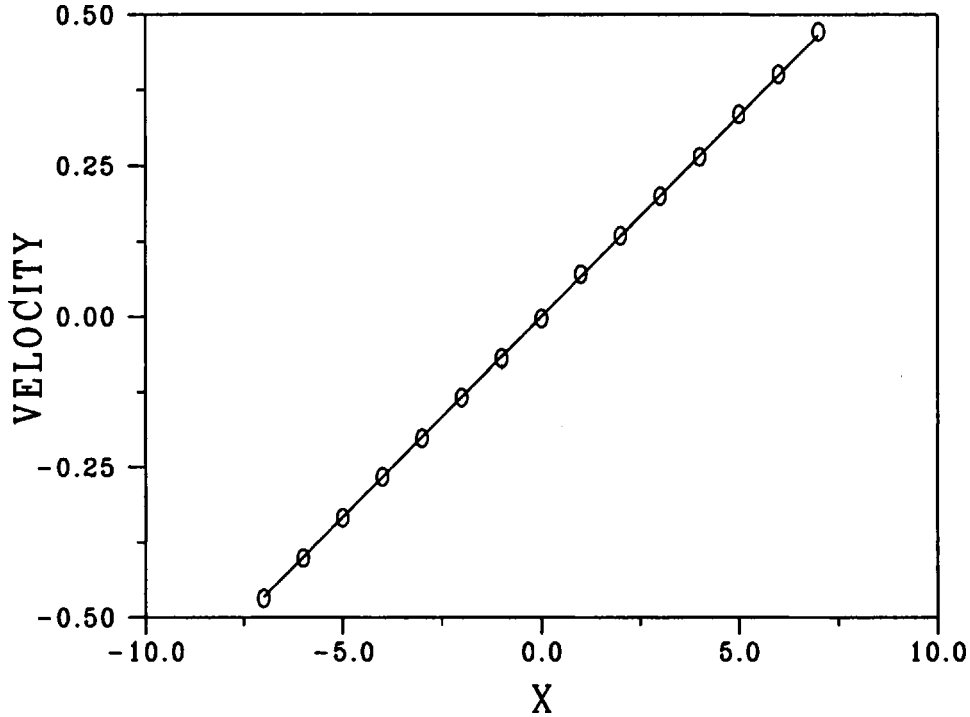


FIG. 1. Couette flow obtained by utilization of the Lees–Edwards boundary condition. The solid line is the theoretical prediction,  $X$  is the position (perpendicular to the vorticity and flow direction) in the simulation cell and the circles are data representing local flow field from the simulation, averaged over 100 time steps.

face, by embedding a cell in the wall that is a mirror image of the adjacent fluid particles but with the velocities in the opposite direction. Although not exact, this is somewhat akin to the bounceback boundary condition used in lattice Boltzmann simulations [Rothman and Zaleski (1994)].

#### IV. APPROXIMATE HARD SPHERE SUSPENSIONS

##### A. Dilute suspensions: Recovery of Einstein intrinsic viscosity

For very dilute to semidilute suspensions, the relative viscosity is described by

$$\eta_r = \eta/\eta_s \approx 1 + \eta_o\phi + K_H\phi^2 + \dots, \quad (14)$$

where  $\eta_r$  is the relative viscosity,  $\eta$  is the viscosity of the suspension,  $\eta_s$  is the viscosity of the fluid solvent (or embedding fluid),  $\eta_o$  is the intrinsic viscosity (equal to 2.5 for suspensions composed of spheres),  $\phi$  is the volume fraction of rigid bodies, and  $K_H$  is the Huggins coefficient. As a simple test, a single sphere with radius  $a=5.511$  was introduced into a well characterized fluid system where the viscosity was known to about one part in a thousand. The simulation cell was  $45^3$  so that adding a single sphere made  $\phi=7.692 \times 10^{-3}$ . At this small solid fraction, only the lowest order term in Eq. (14) is important. Here  $\eta_r \approx 1+2.5\phi=1.0192$ . After shearing this system over 40 times the system size, the DPD simulation obtained  $\eta_r=1.019\pm 0.002$  implying the intrinsic viscosity is  $2.46\pm 0.26$  which is in good agreement with theory. The uncertainty is based on a standard deviation analysis of simulation data.

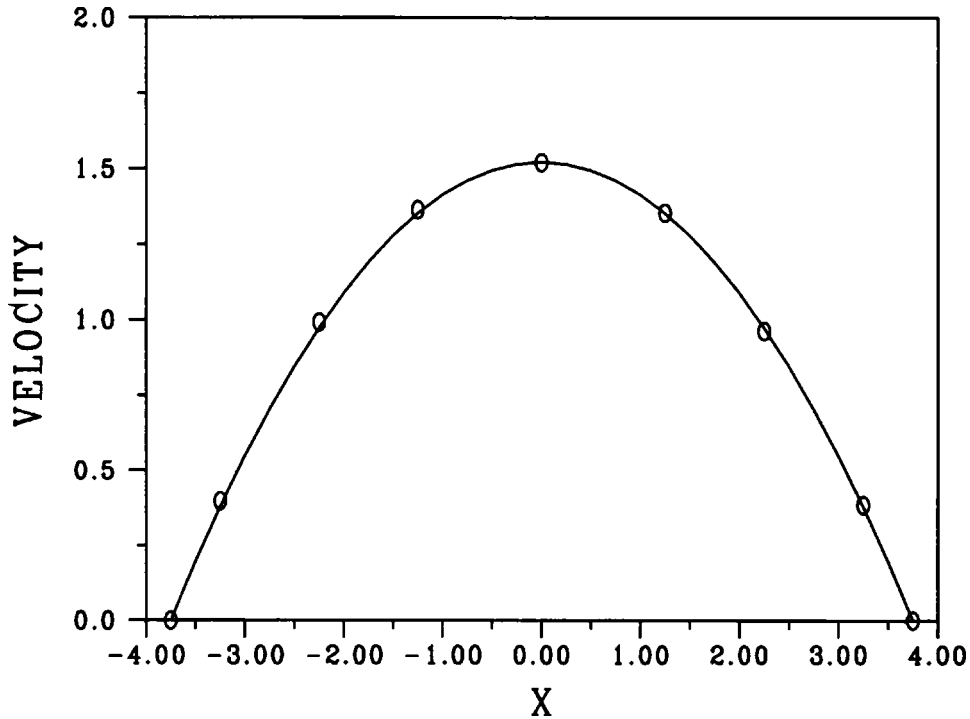


FIG. 2. Poiseuille flow obtained by applying a body force to the DPD fluid. An effective no-slip boundary condition is imposed at the walls.  $X$  is the position relative to the center of the cell. The circles are data representing the average local flow field from the simulation. The value of viscosity determined from a theoretical fit (solid line) for Poiseuille flow was consistent with direct calculation of the stress tensor from the Couette flow simulation in Fig. 1.

### B. Semidilute regime: Huggins coefficient

To determine the Huggins coefficient in Eq. (14), a set of simulations were carried out using 1, 3, 5, 10, 17, and 25 monosize spheres. In this case the highest solid fraction was  $\phi \approx 0.2$ . Figure 3 shows the simulation data and, for comparison, experimental data based on sheared suspensions of silica particles [de Kruif *et al.* (1985)] is included. Clearly the agreement with experiment appears quite good in the regime shown here. The intrinsic viscosity, obtained from the intercept of the vertical axis is consistent with that obtained using a single sphere as described in the previous subsection. The Huggins coefficient, obtained from the slope, is in good agreement with predictions of  $K_H \approx 6$ . Since the Huggins coefficient results from an effective interaction between spheres, this is important confirmation that the code does account reasonably well for longer range hydrodynamic interactions in the fluid.

### C. Dense suspensions: Lubrication forces

At higher volume fractions ( $\phi > 0.4$ ), it became increasingly difficult to carry out simulations without having sphere overlaps occurring. This problem worsened as the Peclet number increased. One reason for overlaps is that the interactions between individual DPD particles are “soft” allowing for some penetration. A simple fix to the code was attempted by including a very steep repulsive interaction between spheres. While such forces greatly suppress the overlaps, it was found that the relative viscosities were,

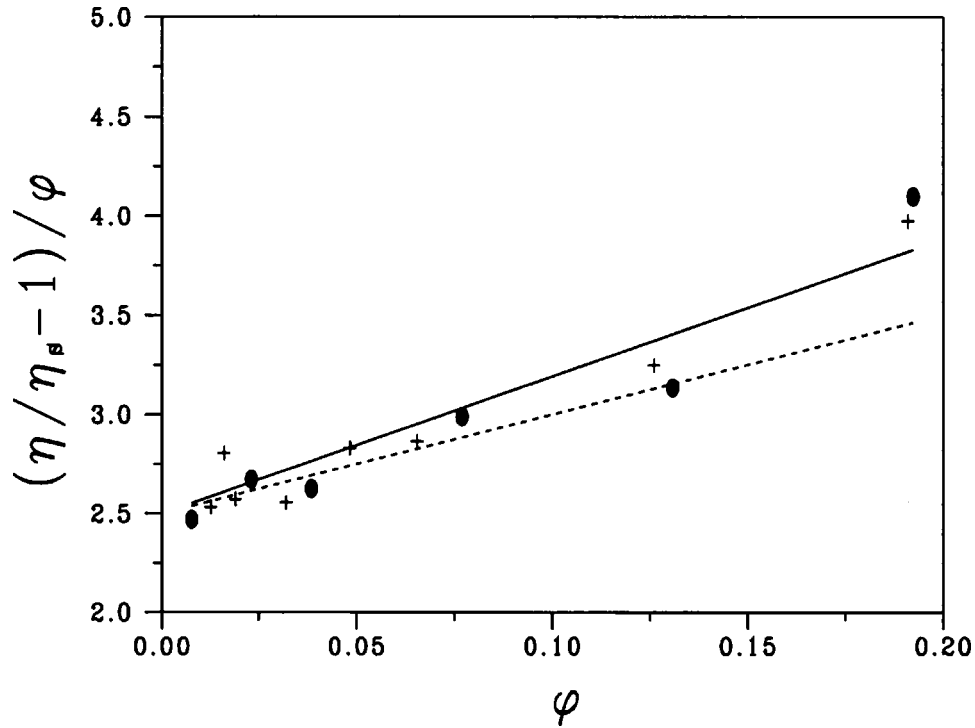


FIG. 3. Determination of the intrinsic viscosity (y intercept) and Huggins coefficient (slope) for a semidilute suspension. The solid circles represent simulation data and the +’s are derived from experiment. The lines correspond to a Huggins coefficient of 7 (solid) and 5 (dashed). Statistical uncertainties in the simulation data were approximately 10% or smaller.

at high  $Pe \approx 10\,000$ , low by a factor of 2 or more when compared to SD or experimental data (Fig. 4). Indeed, these simulation results are roughly akin to the extrapolation of relative viscosity data, from the low to high  $Pe$  number limit, without consideration of lubrication forces. From lubrication theory [Kim and Karrila (1991)], it is well known that the force between approaching spheres, to lowest order, scales as  $(V_A - V_B)/s_{AB}$  where  $V_A$  and  $V_B$  are the velocities of spheres labeled  $A$  and  $B$  and  $s_{AB}$  is the distance between the nearest points of the respective two sphere surfaces {the reader is referred to the literature for further details on lubrication forces [Kim and Karrila (1991)]}. Clearly, as smaller and smaller distances between spheres are probed, lubrication forces are not properly accounted for by the usual DPD interactions, in part because the spatial resolution required is impractical. Hence, it was necessary to directly incorporate the lubrication forces into the DPD code. Here, analytical expressions for the lubrication forces were kept up to first order, (including terms that scale as  $1/s_{AB}$ ,  $\ln s_{AB}$ , and  $s_{AB} \ln s_{AB}$ ). Unfortunately, lubrication theory makes the assumption that the distance between spheres is much smaller than the radius  $a$ , so it is not precisely clear when to turn off the DPD interactions between spheres and when to turn on the lubrication forces. For simulation results presented in this paper, only spheres where  $s_{AB} < a$  were evaluated for lubrication forces. Also, the velocity dependent DPD interparticle interactions between spheres were turned off and an empirical function  $S_f$  was introduced to smoothly incorporate the lubrication forces into the algorithm. For this study, the lubrication forces were multiplied by the following function

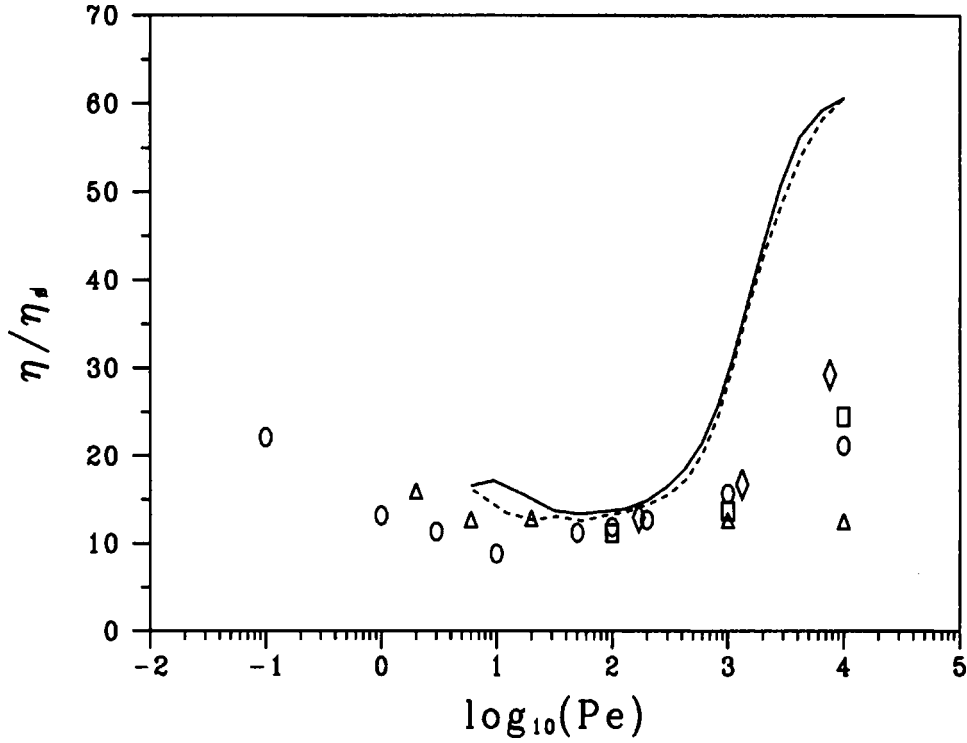
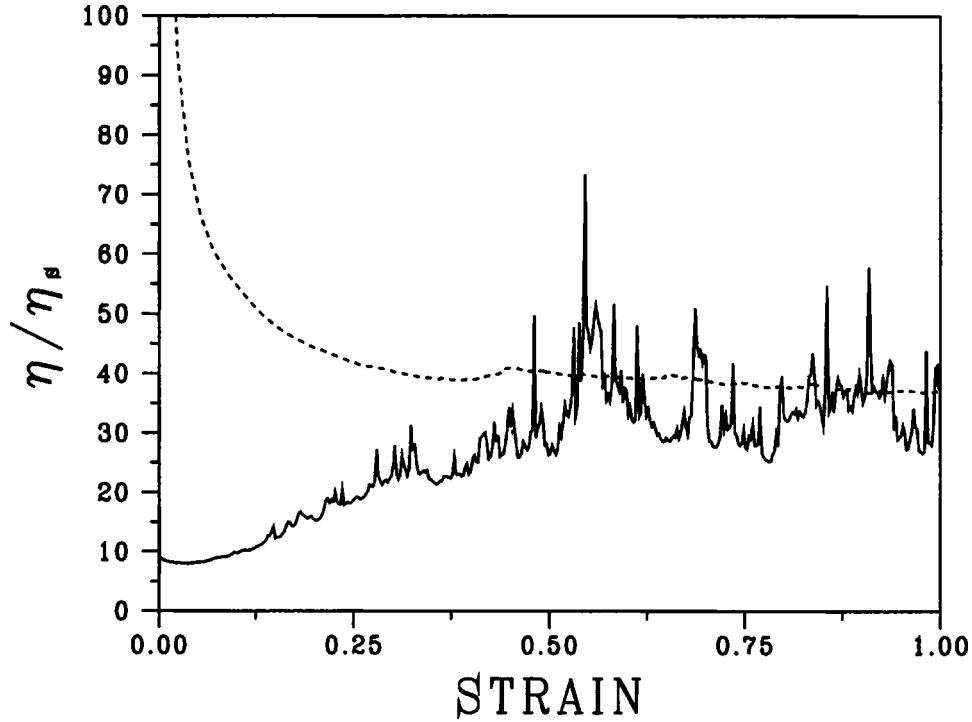


FIG. 4. Comparison of simulation predictions and experimental data for high volume fraction effective hard sphere systems. Here  $\phi=0.49$ . The open circles are results from Stokesian dynamics simulations [Foss and Brady (2000)], open triangles are from DPD simulations without lubrication forces and open squares are from DPD simulations with lubrication forces. The open diamonds are results from the DPD simulation where a constant stress was applied instead of the Lees–Edwards boundary condition. The solid and dashed lines are experimental data from sheared suspensions of silica particles [Bender and Wagner (1996)].

$$S_f = 2/[1 + (s_{AB}/a)^2] - 1. \quad (15)$$

While a “best” choice of smoothing function still needs further study, the form chosen was fairly simple and allows for a close approach to the “true” lubrication force when  $s_{AB} \ll a$ . Indeed, some other forms of smoothing functions were tested, but there was no significant difference in the results. For such dense systems, all neighboring spheres nearly touch and, as a result, the force between them is dominated by its singular nature.

Even with the introduction of the lubrication forces it was difficult, at values of  $Pe \approx 1000$  and greater to avoid some overlap. This was a result of using a constant time step that was not sufficiently small to account for forces when the spheres were in very close proximity to each other. This issue has been noted elsewhere in the literature [Ball and Melrose (1995a, 1995b)]. It is interesting that earlier simulations using SD [Foss and Brady (2000)], with a constant time, allowed for overlaps of about 1% of the sphere radius. When this occurred, a very small separation was assumed (of order  $10^{-8}$  the sphere radius) and the simulation was allowed to progress. This approximation was probably not unreasonable because, at the length scales probed, the forces between the spheres cannot be described by lubrication theory alone. Also, as the spheres approach each other, a slip velocity may become apparent since the mean free path of the fluid atoms will be of order the spacing between sphere surfaces. Consequently, an assumption underlying the derivation of lubrication forces, no slip at fluid/surface boundary, would



**FIG. 5.** Calculated values of relative viscosity as a function of integrated strain rate. The dashed line corresponds to data from a constant stress driven system. The solid line is from a simulation with constant strain rate (Lees–Edwards boundary condition). Note the large temporal fluctuations in relative viscosity for the constant strain rate case as spheres must respond to an unyielding motion resulting from such boundary condition.

need to be modified and there may no longer be a singularity in the force as the spheres touch for actual physical systems. Further research is needed on this issue.

An attempt was made to avoid overlaps by including a dispersive short range interaction potential with an adjustable decay width,  $\lambda$ . Here the hope was that introducing a repulsive force would disperse the spheres enough to avoid overlaps from taking place. Then, by decreasing the decay width, we could probe smaller and smaller distances between spheres to see the effect of the lubrication forces. The following form of a repulsive force, similar to the construction used by Foss and Brady (2000), was chosen:

$$\mathbf{F}_{AB} = \frac{Z \exp\left(-\frac{s_{AB}}{\lambda}\right)}{1 - \exp\left(-\frac{s_{AB}}{\lambda}\right)} \hat{r}_{AB}, \quad (16)$$

where  $Z$  is a constant,  $\lambda$  is the decay width, and  $\hat{r}_{AB}$  is a unit vector pointing from the center of sphere  $A$  to sphere  $B$ . Not unexpectedly, it was found that the viscosity was sensitive to  $\lambda$  and increased with decreasing  $\lambda$ . For one set of simulations, 27 spheres were used with  $\phi=0.477$  and  $Pe \approx 1000$ . Here the suspension was sheared with a strain equivalent to over ten simulation cells for cases of  $\lambda/a \approx 8.0 \times 10^{-5}$ ,  $2.0 \times 10^{-5}$ , and  $4.0 \times 10^{-6}$ . The relative viscosity was 8.58, 10.1, and 11.1, respectively. In this case, no overlaps occurred as the spheres managed to squeeze by each other, although coming quite close, with the ratio of the distance between sphere centers to diameter equal to

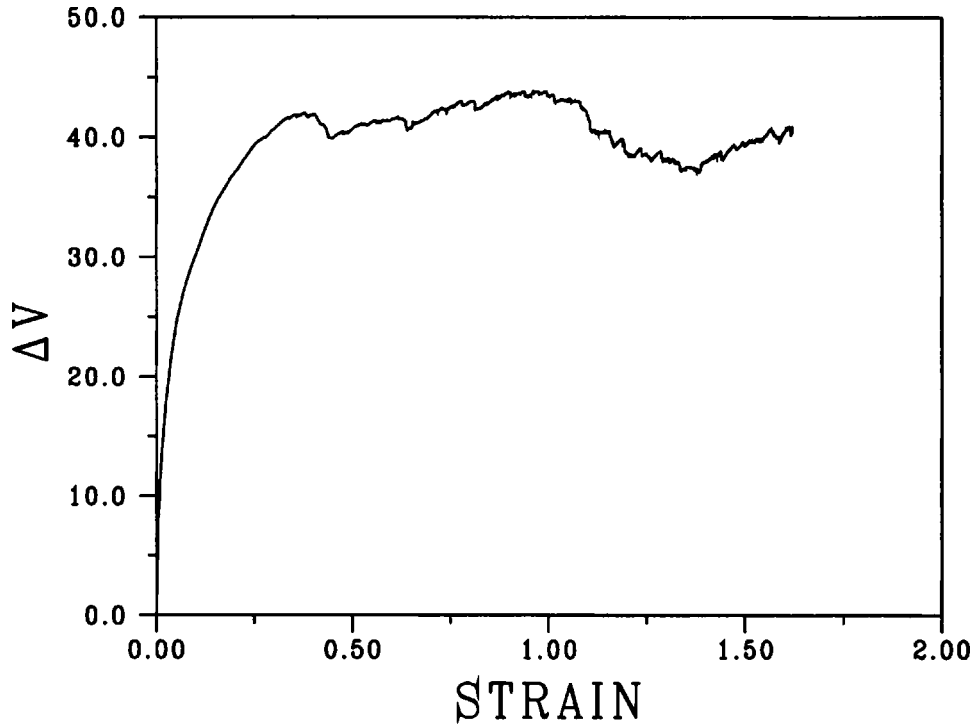


**FIG. 6.** Constant stress driven shear. The velocity difference of the two parallel regions where the force is applied is given by  $\Delta V$ . To set the velocity scale,  $\Delta V=40$  corresponds to  $Pe \approx 10\,000$ . For this system  $\phi \approx 0.49$ . There were moderate fluctuations in  $\Delta V$  as the simulation progressed.

1.000 000 01 and smaller. However a second set of simulations was carried out with the sphere radius about 1% larger, making  $\phi=0.49$ . The same set of  $\lambda/a$  was used. This time, despite the relatively small increase in sphere radius, the time step needed for the simulation to proceed without overlaps, was too small to be practical.

Instead of relying on a dispersive force to help separate the spheres, it was then decided that the best route would be to incorporate a variable time step into the code. A simple modification was made to the algorithm such that, as the spheres approached each other, the time step was reduced by a factor of 5 if the sphere's projected trajectory appeared close to creating an overlap. A suspension of 663 spheres was simulated with volume fraction 0.49. It was found that at  $Pe=1000$  the system evolved in a relatively smooth fashion but at higher  $Pe \approx 10\,000$  large fluctuations were found in the stress. As the viscosity is related to stress [see Eq. (13)] it would also appear as if the viscosity was dramatically fluctuating (see Fig. 5). Recently, in experimental studies of constant strain rate driven dense suspensions [Lootens *et al.* (2003)], large fluctuations in the stress have been observed. The large fluctuations have been related to the onset of a jamming transition. What was not clear from the simulations was whether the onset of the larger fluctuations in the measured viscosity was a consequence of the constant strain rate boundary condition when employing the Lees–Edwards boundary condition. As an alternative to the Lees–Edwards boundary condition, a simulation was set up so that an applied stress was used to drive the system. Here two narrow bands of spheres were constrained to move in parallel planes having a spacing of about four sphere diameters between each other. A force was applied on the spheres, in opposite directions in each

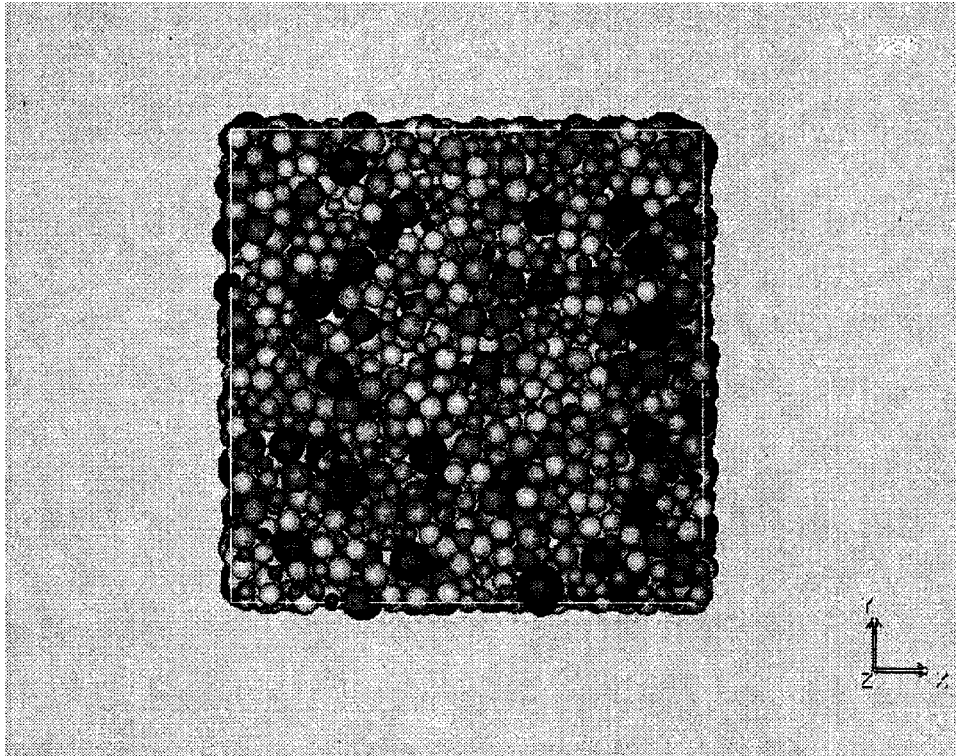


FIG. 7. Suspension of polydisperse spheres with  $\phi=0.55$  and  $\sigma=0.2$ .

separate plane, so that a shearing motion was established. The simulation cell contained 340 spheres. Figure 6 shows the average velocity difference  $\Delta V$  between the top and bottom bands of spheres as a function of integrated strain. In this case, the resulting strain rate is no longer constant with the average velocity varying about 5%–10%. Clearly, temporal fluctuations in the measured viscosity were greatly reduced for the constant stress case (see Fig. 5). On the other hand, the average viscosity determined from the stress controlled simulation was about 10%–30% higher than the strain controlled simulation in this high Pe regime. Since the gap between plates was about four sphere diameters, finite size effects could have made the relative viscosity appear higher. A related observation was made by Boek and van der Schoot (1998) concerning finite size and resolution effects. Here it was found that, at low Pe, estimates of the relative viscosity improved (when compared to experimental values) when the colloidal spheres were made sufficiently small. Unfortunately, it was not clear if this was a consequence of having smaller spheres relative to the simulation box size alone (a finite size effect), or, in part, the result of a repulsive force between particles helping better disperse the spheres and reduce overlaps (a resolution effect). Such finite size effects will be the subject of future research.

For  $Pe=10\,000$  the relative viscosity was, for the constant strain rate case, about 10% higher than that of previous Stokesian dynamics simulations (see Fig. 4). Although within the statistical uncertainty, it is possible that the correction for the overlaps in the SD simulations was in part the cause of the discrepancy as can be seen from the above study of dispersed spheres. Allowing for the smaller distances between spheres (i.e., as  $\lambda/a$  is decreased) would have probably increased the viscosity in the high Pe case. Finally, using

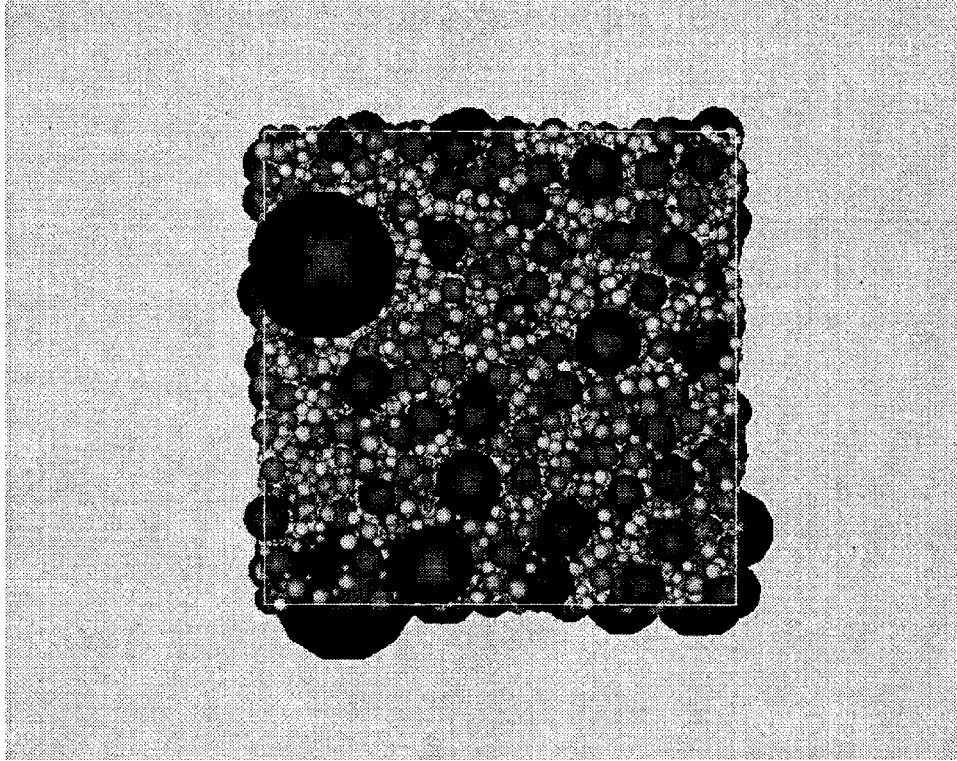


FIG. 8. Suspension of polydisperse spheres with  $\phi=0.55$  and  $\sigma=0.8$ .

a variable time step does not guarantee, for some unique configuration of spheres and flow history, that the time step may again become too small to be practical. However, this problem is not necessarily the same as jamming, where the system cannot move without overlaps, but more a case of developing a reasonable strategy for updating the sphere positions.

Figure 4 contains experimental data from a stress controlled measurement of a sheared silica suspension due to Bender and Wagner (1996). The agreement with our stress controlled simulation is good in regards to capturing trends. However, one needs to take great care when comparing simulations of such an idealized system to experiments (and vice versa). Interestingly, the silica particles were slightly polydisperse so that one might think the experimental measurements of viscosity would be a bit low, perhaps up to 10% or so at this volume fraction, relative to a monosize sphere case (see section on polydispersivity). Unfortunately, such corrections for polydispersivity would make agreement worse. Second, the data shown and other comparable experimental data {e.g., spherical silica particles [Bender and Wagner (1996)] and poly(methylmethacrylate) (PMMA) [D'Hane *et al.* (1993); Phan *et al.* (1996)]} are based on measurements of suspension with particles approximately 100–1000 nm in diameter. Again, consider the earlier set of simulations where a dispersive force was introduced. As the width of the potential  $\lambda/a$  ranged from 0.0001 to 0.000 004 the viscosity was not quite at its asymptotic limit (also note  $Pe \approx 1000$ ). Probing the experimental particles at similar  $\lambda/a$  (and at higher  $Pe$ ) would put one at atomic scales and smaller. Clearly at such length scales the silica and PMMA particles are not exactly hard spheres and the embedding fluid can no longer be

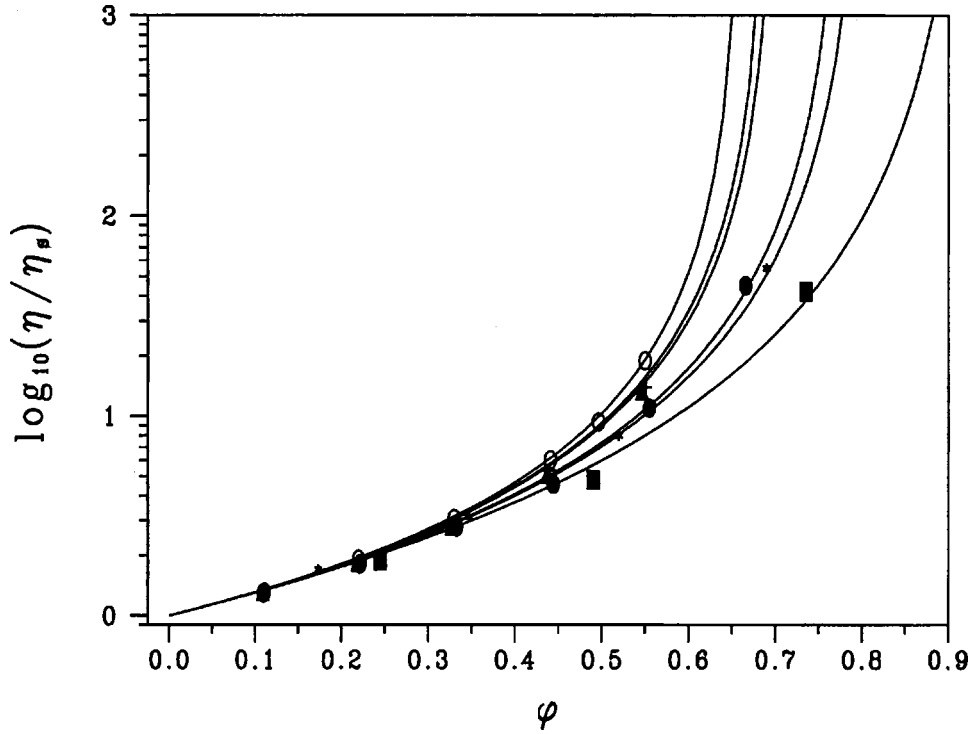


FIG. 9. Relative viscosity of polydisperse suspensions. Shown are simulation data for  $\sigma_{\text{rms}}=0, 0.2, 0.4, 0.6, 0.8,$  and  $1.0$ . Solid lines are fits of data to Krieger–Dougherty equation. Curves offset to the right correspond to increasing  $\sigma_{\text{rms}}$ . Statistical uncertainties in the simulation data were approximately 10% or smaller.

represented as a continuum. So it is not clear if the experiments in the high  $Pe > 1000$  can be modeled as hard sphere fluids without consideration of these features. A related observation was made by Ball and Melrose (1995b) who described their simulation results as unphysical with respect to modeling colloidal systems when such small distances were probed.

#### D. Polydispersivity

The role of size distribution of spherical shaped aggregates on relative viscosity was examined. An approximate log normal distribution was used and sphere size distributions were characterized by the mean squared deviation of sphere radii, normalized to the average sphere radius,  $\sigma_{\text{rms}}$ , that is given by

$$\sigma_{\text{rms}}^2 = \frac{1}{\langle a \rangle^2} \sum_{i=1,N} (a_i - \langle a \rangle)^2 f_i, \quad (17)$$

where  $f_i$  is the volume fraction of spheres with radius  $a_i$  (normalized by the total volume of spheres) and  $\langle a \rangle$  is a similarly weighted average sphere radius. We allowed  $\sigma_{\text{rms}}$  to range from 0 to 1 (Figs. 7 and 8). For  $\sigma_{\text{rms}}=0$ , the spheres are monosize and when  $\sigma_{\text{rms}}=1$  the spheres size varied by a factor of about 30. In this study, the focus was more on the role of size variation and it was decided to not include lubrication forces in the simulation as very small time steps would be needed, making the simulation too time consuming. Hence, only a moderate  $Pe \approx 10$  was considered.

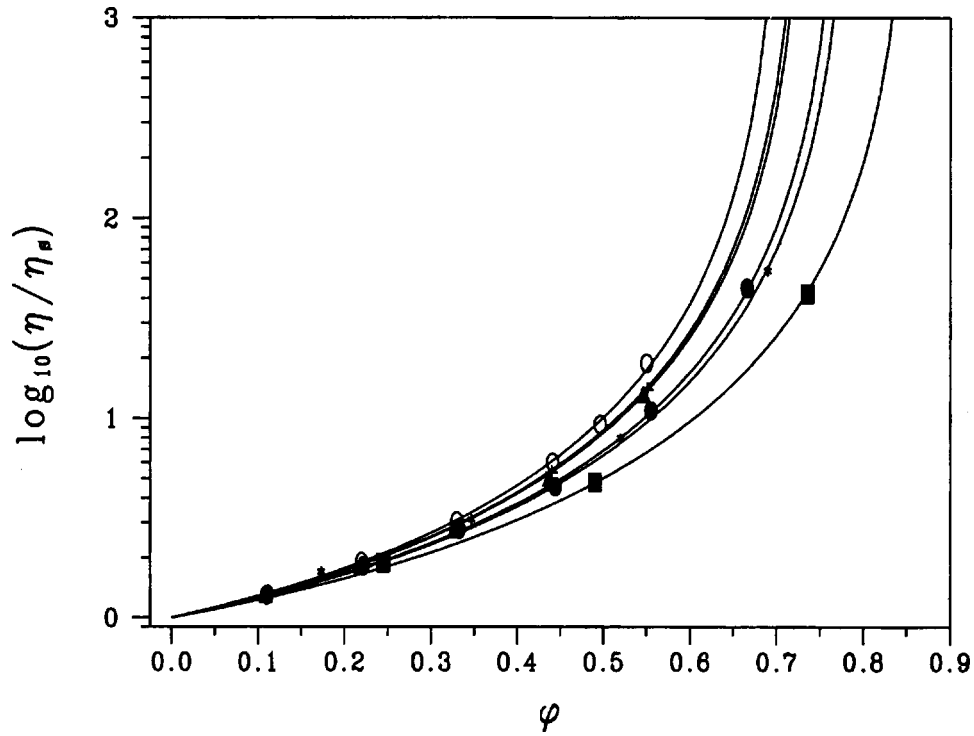


FIG. 10. Fit of same data in Fig. 8 to Eq. (21) with  $n=2$  and terms up to  $K_2$  retained. Statistical uncertainties in the simulation data were approximately 10% or smaller.

In these simulations the suspension was sheared using the Lees–Edwards boundary condition. The stresses in the system were then calculated and the viscosity determined using Eqs. (12) and (13). Figure 9 shows the relative viscosity as a function of solid fraction for different values of  $\sigma$ . Note that at low solid fractions the data did not appear very sensitive to the value of  $\sigma_{\text{rms}}$ . This is, in part, an artifact of plotting our data on a log scale, although it was not expected that there would be a large difference in this regime. However, as the solid fraction increases the relative viscosity, at the same  $\phi$ , clearly decreased with increasing  $\sigma_{\text{rms}}$ . This can be understood as a consequence of the maximum packing  $\phi_c$  of the sphere system increasing as the particle size distribution becomes wider.

One of the most well known equations for fitting relative viscosity data, for a broad range of  $\phi$ , is the Krieger–Dougherty (KD) equation [Krieger and Dougherty (1959)]. The KD equation is based on effective medium theory arguments. Here, incremental changes to the solid volume fraction of a suspension increases the viscosity as if small particles were being added to the suspension, which is treated as a homogeneous viscous medium. In addition, a correction is needed to allow the viscosity to diverge at  $\phi_c$ . The KD equation has the following form:

$$\eta/\eta_s = \left(1 - \frac{\phi}{\phi_c}\right)^{-\eta_0\phi_c}. \quad (18)$$

Fits to the KD equation were reasonable and are shown in Fig. 9. Consider the expansion of the KD equation in terms of  $\phi$ :

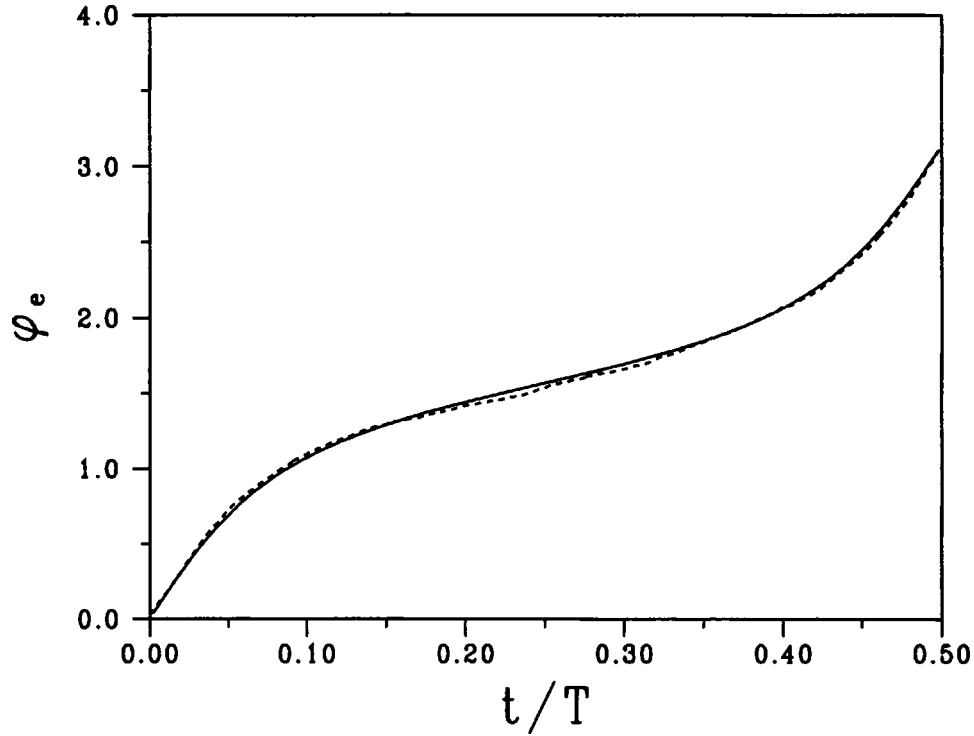


**FIG. 11.** Comparison of DPD simulation (dashed line) to predictions from theory (solid line) for rotation of prolate spheroid under shear. Here,  $\phi_e$  is the angle of orientation,  $t$  is the time, and  $T$  is the period of rotation [Eq. (23)].

$$\eta/\eta_s = 1 + \eta_o\phi + \frac{\phi_o}{2} \frac{\eta_o\phi_c + 1}{\phi_c} \phi^2 + \dots \quad (19)$$

By construction, the KD equation obtains the correct intrinsic viscosity. For polydisperse sphere systems, the KD equation would predict that the Huggins coefficient varies from approximately 5.08 to 4.375 as  $\phi_c$  increases from 0.64 to 1. Theoretical work [Wagner and Woutersen (1994)] shows  $K_H$  weakly depends on the polydispersivity of spheres in a suspension. For example, it was found that  $K_H$  was reduced by about 13% for suspensions where the ratio of maximum to minimum radii was about 10. One might find troubling the increase of the exponent,  $1.6 \leq \eta_o\phi_c \leq 2.5$ , describing the divergence of viscosity as  $\phi_c$  is approached from below. Some experimental results point to a divergence of viscosity with a critical exponent of 2 [de Kruif *et al.* (1985)]. Regardless, the KD equation captures the main trends correctly although the value of  $K_H$  and the critical exponent are not exact.

Bicerano *et al.* (1999) suggested the following equation, which was intended to describe a suspension with uniform sized spheres and a maximum random packing fraction  $\phi_c=0.64$ :

$$\eta/\eta_s = \left(1 - \frac{\phi}{\phi_c}\right)^{-2} \left[1 - 0.4 \frac{\phi}{\phi_c} + 0.34 \left(\frac{\phi}{\phi_c}\right)^2\right]. \quad (20)$$

By construction, it recovers the Einstein intrinsic viscosity and a Huggins coefficient of

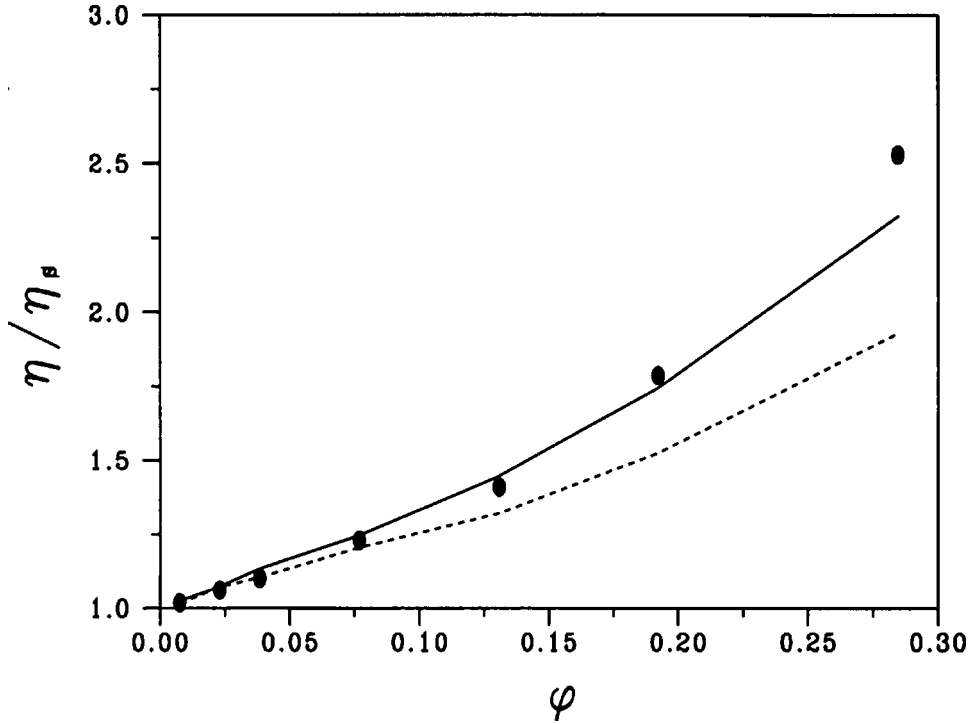
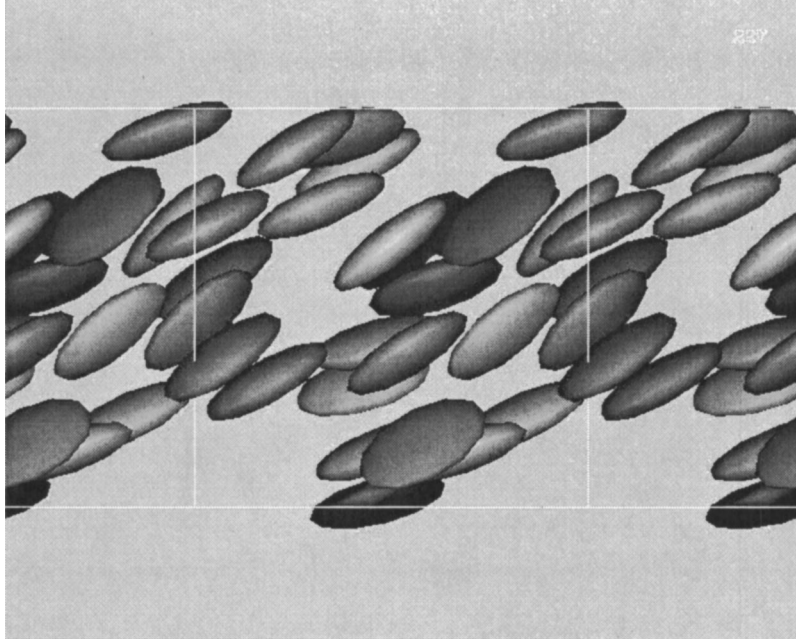


FIG. 12. Relative viscosity for spheroid systems. Shown are data for oblate (dashed line), spherical (filled circles), and prolate (solid line) spheroids. Note that at  $\phi \approx 0.1$  of rate of increase of relative viscosity with  $\phi$  for the oblate spheroid decreases, indicative of the onset of an apparent nematic phase. A nematic phase for the prolate spheroids occurs at somewhat higher  $\phi$ . Statistical uncertainties in the simulation data were approximately 10% or smaller.

$K_H=6.2$  while fixing the critical exponent to the value 2. Equation (20) can be generalized for suspensions composed of particles with arbitrary shape and size distributions

$$\eta/\eta_s = \left(1 - \frac{\phi}{\phi_c}\right)^{-n} \left[1 + K_1 \frac{\phi}{\phi_c} + K_2 \left(\frac{\phi}{\phi_c}\right)^2 + \dots\right], \quad (21)$$

where  $n$  is the critical exponent describing the divergence of the viscosity as the critical packing is approached and  $K_1 = \phi_c^2 \eta_0 - n$  and  $K_2 = \phi_c^2 K_H - n \phi_c \eta_0 + n(n-1/2)$  are chosen to match the intrinsic viscosity and Huggins coefficient for that suspension, respectively [note, the generalization of Eq. (20) was done in collaboration with Flatt]. In principle, such terms can also be generalized to account for a shear dependence and interparticle interactions. The intrinsic viscosity is known for many shapes [Douglas and Garboczi (1995)] and  $K_H$  is predicted as a function of polydispersity of sphere systems [Wagner and Woutersen (1994)]. For arbitrarily shaped objects, one could determine  $\eta_0$  and  $K_H$  by simulations in the regime where  $0 < \phi < 0.15$ . Higher order terms proportional to  $\phi^3$  and so forth may become important as the volume fraction is increased although at some point the singular term should dominate. Also, it is not clear if the critical exponent  $n$  is truly universal. The value of 2 used in Eq. (20) is based on a formal hydrodynamic-electrostatic analogy of suspensions. In this analogy,  $n$  is equal to the percolation theory insulator exponent, which has a value close to 2 in three dimensions. Off lattice models can give rise to different values of  $n$  so that the universality of this exponent may only be



**FIG. 13.** Evidence of an apparent nematic phase for the oblate spheroid system with  $r_e=1/3.28$ . The particles initial orientation was such that the axis of symmetry was in the vorticity direction (perpendicular to the page). Here, the Jeffery's orbits were suppressed.

approximate [Feng *et al.* (1987)]. Regardless, precise determination of a critical exponent from simulation would require a finite size scaling study that is beyond our current computational capabilities. Figure 10 shows the same data as in Fig. 9 but fit with Eq. (21) with the constraint that the critical exponent  $n=2$ .

## V. JEFFERY'S ORBIT FOR SPHEROIDAL SYSTEMS

Jeffery showed that ellipsoids of revolution rotate in a linear shear field with a period

$$T = 2\pi(r_e + 1/r_e)/\dot{\gamma}, \quad (22)$$

where  $r_e$  is the ratio between the major and minor axis of an ellipsoid of revolution. This prediction has been validated by experiment [cf. Zia *et al.* (1967)]. To determine whether a DPD based code could recover this result, an ellipsoid of revolution was approximated by creating a template of DPD particles that fall within the boundaries of an prolate ellipsoid of revolution with  $r_e=2.4$ . The simulation had Reynolds number  $Re < 1$  and the value of  $Pe$  (of order 1000) high so that inertial and diffusive effects could be minimized. It was found that the simulation obtained a period with less than 2% error when compared to that predicted by Jeffery's theory. Figure 11 shows a comparison of simulation results and the prediction of Jeffery, for the rotational orientation of the spheroid, as a function of time. Here, the rotational orientation of the ellipsoid of revolution is given by [Larson (1999); Eirich (1967)]:

$$\tan \phi_e = r_e \tan(2\pi t/T). \quad (23)$$

The relative viscosity as a function of  $\phi$  was then determined for three spheroid systems: monosize spheres, oblate ( $r_e=1/3.28$ ) ellipsoids of revolution, and prolate ( $r_e=2.4$ )

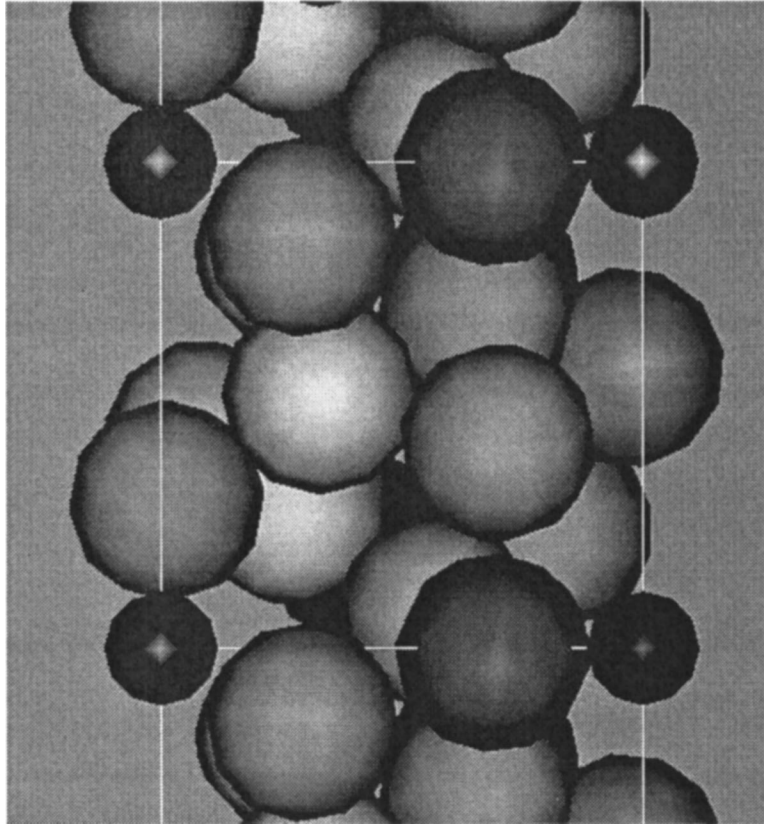


**FIG. 14.** Flow through rebars: Case A. A suspension of spheres was subject to a body force downward. The sphere's diameter was about  $\frac{1}{2}$  the gap spacing between the rebars (the four smaller radii objects represent cylinders). The volume fraction was  $\phi \approx 50\%$ . After a short period, the flow came to a stop as the spheres became jammed between the rebars.

ellipsoids of revolution (Fig. 12). For each shape particle, simulations were carried out for 1, 3, 5, 10, 17, and 25 rigid bodies. In all the simulations, the volume of the individual rigid bodies were nearly equal. As the system was sheared, Jeffery orbits were clearly seen at the lowest volume fractions (a few spheroids). However, for the case of oblate spheroids, between  $\phi=0.10$  and  $0.15$  the Jeffery orbits became suppressed and an apparent nematic phase [Larson (1999)] or orientational order (Fig. 13) was observed. At these solid fractions some prolate spheroids were still undergoing Jeffery orbits. It was not until the higher solid fractions were reached that the the prolate spheroids became more aligned. It is likely that the oblate spheroids ordered at the lower volume fraction because they are somewhat flatter, with a relatively large and round cross section, than the prolate spheroids, making it more difficult to “squeeze” out the fluid between them as they try to undergo Jeffery orbits near each other. Accompanying the nematic phase was an apparent reduction in the rate of increase of the relative viscosity. Indeed, as can be seen in Fig. 12 the relative viscosity for the oblate spheroids was lower than the relative viscosity of the spheres when  $\phi \gtrsim 0.015$ . It should be pointed out that in these simulations, lubrication forces were not included and, because of the periodicity of the system, the ordering could have been enhanced. So, further study is needed to see whether these results apply to larger systems and to fully understand the effect of lubrications forces.

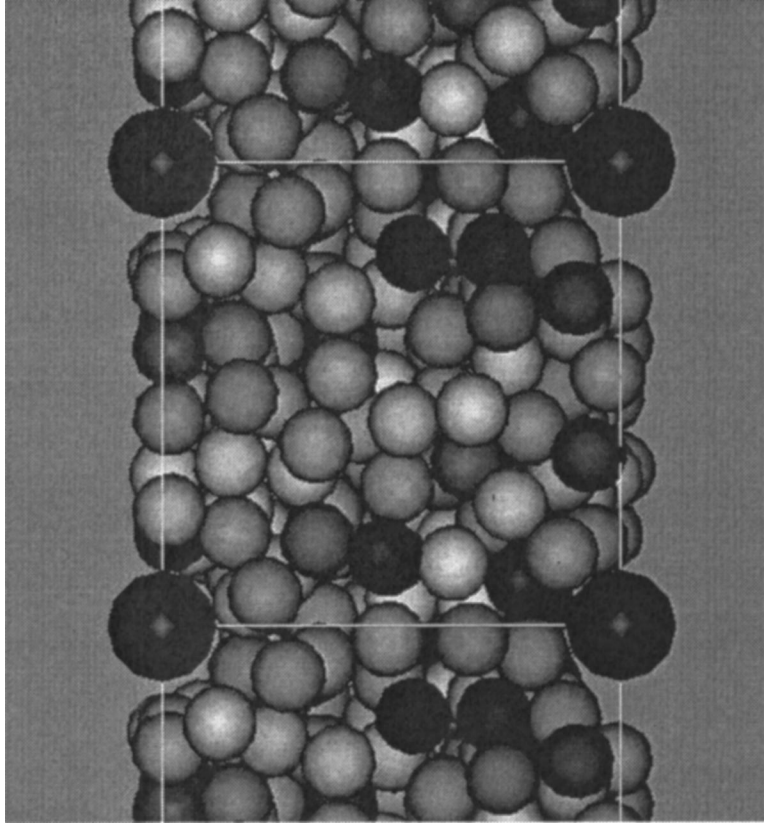


**FIG. 15.** Flow through rebars: Case B. Here the sphere diameters were about  $\frac{1}{5}$  the gap spacing. The volume fraction was  $\approx 50\%$ . The spheres continued to flow throughout the simulation, which ran several times longer in time than in case A. There was no indication of jamming (note, lubrication forces were not included in this simulation).

## VI. FLOW IN OTHER GEOMETRIES

A nice aspect of DPD is its flexibility in modeling flow in other complicated (non-Couette-like) geometries of interest. Such simulations can help provide insight into the important physical mechanisms controlling flow and are useful for the interpretation of measurements. As a simple illustration, consider the flow of a suspension, driven by a body force, between parallel cylinders. This flow scenario is actually quite common when, for example, fresh concrete is poured such that it flows between rebars, which are cylindrical steel bars that are often oriented in a parallel fashion. Figures 14 and 15 shows two cases where in case A the sphere diameter was about  $\frac{1}{2}$  the gap spacing between the rebars. For case B, the sphere diameters were about  $\frac{1}{5}$  the gap spacing. A body force was applied so that the flow was downward. As the simulations progressed, for case A the flow stopped as the spheres became jammed between the rebars. In case B, the simulation showed no indication of jamming. It should be pointed out that, as a practice in the concrete industry, the size of coarse aggregates should be less than a third of the gap spacing between rebars to avoid this very phenomenon. Practice is clearly ahead of theory on this issue.

## VII. CONCLUSION

In this paper, results from a study testing a DPD based simulation technique for modeling suspensions were presented. It is concluded that DPD can be used as an alternative computational tool for modeling a fairly wide variety of suspensions. Without significant modification, the method recovers well established predictions concerning the flow of a suspension for volume fractions in the dilute to semidilute systems regime. At higher volume fractions and  $Pe$ , modifications, such as a variable time step and explicit inclusion of lubrication forces are necessary to account for important phenomena that must be resolved at small time and length scales. This should also be true for other approaches like numerical solution of the Navier–Stokes equations at a similar resolution. Indeed, similar modifications have been employed for a lattice Boltzmann [Nguyen and Ladd (2002)] based model of suspensions. Further validation would be useful, e.g., testing how well the model describes sedimentation.

## ACKNOWLEDGMENTS

The author would like to thank Robert Flatt for providing the sphere size distributions used in the polydispersivity study and James Sims and Willian George for working on the parallel implementation of the code. The author would also like to thank Andreas Acrivos, John Brady, Jack Douglas, German Drazer, Ray Mountain, and Norman Wagner for useful conversations. This work was supported by the Virtual Cement and Concrete Testing Laboratory (VCCTL) consortium, the Center for Advanced Cement Based Materials (ACBM), and the HYPERCON program at the National Institute of Standards and Technology.

## References

- Allen, M. P., and D. J. Tildesley, *Computer Simulation of Liquids* (Clarendon, Oxford, 1987).
- Ball, R. C., and J. R. Melrose, "The pathological behaviour of sheared hard spheres with hydrodynamic interactions," *Europhys. Lett.* **32**, 535–540 (1995a).
- Ball, R. C., and J. R. Melrose, "Lubrication breakdown in hydrodynamic simulations of concentrated colloids," *Adv. Colloid Interface Sci.* **59**, 19–30 (1995b).
- Bender, J., and N. J. Wagner, "Reversible shear thickening in monodisperse and bi disperse colloidal dispersions," *J. Rheol.* **40**, 899–916 (1996).
- Bicerano, J., J. F. Douglas, and D. A. Brune, "Model for the viscosity of particle dispersions," *J. Macromol. Sci., Rev. Macromol. Chem. Phys.* **C39**, 561–642 (1999).
- Boek, E., P. V. Coveney, H. N. Lekkerkerker, and P. van der Schoot, "Simulating the rheology of dense colloidal suspensions using dissipative particle dynamics," *Phys. Rev. E* **55**, 3124–3133 (1997).
- Boek, E., and P. van der Schoot, "Resolution effects in dissipative particle dynamics simulations," *Int. J. Mod. Phys. C* **9**, 1307–1318 (1998).
- Brady, J. F., and G. Bossis, "Stokesian dynamics," *Annu. Rev. Fluid Mech.* **20**, 111–157 (1988).
- de Kruif, C. G., E. M. F. van Lersel, A. Vrij, and W. B. Russel, "Hard sphere colloidal dispersions: Viscosity as a function of shear rate and volume fraction," *J. Chem. Phys.* **83**, 4717–4725 (1985).
- D'Haene, P., J. Mewis, and G. G. Fuller, "Scattering dichroism measurements of flow-induced structure of a shear thickening suspension," *J. Colloid Interface Sci.* **156**, 350–358 (1993).
- Douglas, J. F., and E. J. Garboczi, "Intrinsic viscosity and the polarizability of particles having a wide range of shapes," *Adv. Chem. Phys.* **91**, 85–153 (1995).

- Dzwiniel, W., and D. Yuen, "A two-level, discrete particle approach for large-scale simulation of colloidal aggregates," *Int. J. Mod. Phys. C* **11**, 1037–1061 (2000).
- Dzwiniel, W., and D. Yuen, "Mesoscopic dispersion of colloidal agglomerate in complex fluid modeled by a hybrid fluid particle model," *J. Colloid Interface Sci.* **247**, 463–480 (2002).
- Eirich, F., *Rheology: Theory and Application* (Academic, New York, 1967), Vol. 4.
- Español, P., "Fluid particle model," *Phys. Rev. E* **57**, 2930–2948 (1998).
- Español, P., and M. Revenga, "Smoothed particle dynamics," *Phys. Rev. E* **67**, 026705 (2003).
- Español, P., and M. Serrano, "Thermodynamically admissible form of discrete hydrodynamics," *Phys. Rev. Lett.* **83**, 4542–4545 (1999).
- Español, P., and P. Warren, "Statistical mechanics of dissipative particle dynamics," *Europhys. Lett.* **30**, 191–196 (1995).
- Feng, S., B. Halperin, and P. N. Sen, "Transport-properties of continuum systems near the percolation threshold," *Phys. Rev. B* **35**, 197–214 (1987).
- Flekkøy, E. G., P. V. Coveney, and G. D. Fabritius, "Foundations of dissipative particle dynamics," *Phys. Rev. E* **62**, 2140–2157 (2000).
- Foss, D. R., and J. F. Brady, "Structure, diffusion and rheology of brownian suspensions by stokesian dynamics simulation," *J. Fluid Mech.* **407**, 167–200 (2000).
- Groot, R. D., and P. B. Warren, "Dissipative particle dynamics: Bridging the gap between atomistic and mesoscopic simulation," *J. Chem. Phys.* **107**, 4423–4435 (1997).
- Hoogerbrugge, P. J., and J. M. V. A. Koelman, "Simulating microscopic hydrodynamic phenomena with dissipative particle dynamics," *Europhys. Lett.* **19**, 155–160 (1992).
- Jeffery, G. B., "The motion of ellipsoidal particles immersed in a viscous fluid," *Proc. R. Soc. London, Ser. A* **102**, 161–179 (1922).
- Kim, S., and S. J. Karrila, *Microhydrodynamics, Principles and Selected Applications* (Butterworth-Heinemann, Stoneham, MA, 1991).
- Koelman, J. M. V. A., and P. J. Hoogerbrugge, "Dynamic simulation of hard sphere suspensions under steady shear," *Europhys. Lett.* **21**, 363–368 (1993).
- Krieger, I. M., and T. J. Dougherty, "A mechanism for non-newtonian flow in suspensions of rigid spheres," *Trans. Soc. Rheol.* **20**, 137–152 (1959).
- Ladd, A. J. C., "Sedimentation of homogeneous suspensions of non-Brownian spheres," *Phys. Fluids* **9**, 491–499 (1997).
- Larson, R. G., *The Structure and Rheology of Complex Fluids* (Oxford University Press, New York, 1999).
- Lootens, D., H. V. Damme, and P. Hébraud, "Giant stress fluctuations at the jamming transition," *Phys. Rev. Lett.* **90**, 178301 (2003).
- Marsh, C., G. Backx, and M. H. Ernst, "Static and dynamic properties of dissipative particle dynamics," *Phys. Rev. E* **56**, 1676–1691 (1996).
- Marsh, C., G. Backx, and M. H. Ernst, "The Fokker–Planck–Boltzmann equation for dissipative particle dynamics," *Europhys. Lett.* **38**, 441–415 (1997).
- Martys, N. S., and R. D. Mountain, "Velocity Verlet algorithm for dissipative-particle-based models of suspensions," *Phys. Rev. E* **59**, 3733–3736 (1999).
- Monaghan, J. J., "Smoothed particle hydrodynamics," *Annu. Rev. Astron. Astrophys.* **30**, 543–574 (1992).
- Nguyen, N.-Q., and A. J. C. Ladd, "Lubrication corrections for lattice boltzmann simulations of particle suspensions," *Phys. Rev. E* **66**, 046708 (2002).
- Omelyan, I., "On the numerical integration of motion for rigid polyatomics: the modified quaterion approach," *Comput. Phys.* **12**, 97–103 (1998).
- Phan, S., W. B. Russel, Z. Cheng, J. Zhu, P. Chaikin, J. H. Dunsmuir, and R. Ottewill, "Phase transition, equation of state, and limiting shear viscosities of hard sphere dispersions," *Phys. Rev. E* **54**, 6633–6645 (1996).
- Phung, T. N., and J. F. Brady, "Stokesian dynamics simulation of Brownian suspensions," *J. Fluid Mech.* **313**, 181–207 (1996).
- Rothman, D. H., and S. Zaleski, "Lattice-gas model of phase separation, interfaces, phase transitions, and multiphase flow," *Rev. Mod. Phys.* **66**, 1417–1479 (1994).

- Serrano, M., and P. Español, "Thermodynamically consistent mesoscopic fluid particle model," *Phys. Rev. E* **64**, 046115 (2001).
- Sierou, A., and J. F. Brady, "Accelerated stokesian dynamics simulations," *J. Fluid Mech.* **448**, 115–146 (2001).
- Sims, J. S., and N. S. Martys, "Simulation of sheared suspensions with a parallel implementation of *qdpd*," *J. Res. Natl. Inst. Stand. Technol.* **109**, 267–277 (2004).
- Vattulainen, I., M. Karttunen, G. Besold, and J. M. Polson, "Integration schemes for dissipative particle dynamics simulations: From softly interacting systems toward hybrid models," *J. Chem. Phys.* **116**, 3967–3979 (2002).
- Verlet, L., "Computer 'experiments' on classical fluids. I. Thermodynamical properties of Lennard–Jones molecules," *Phys. Rev.* **159**, 98–103 (1967).
- Wagner, N. J., and A. T. J. Woutersen, "The viscosity of bimodal and polydisperse suspensions of hard-spheres in the dilute limit," *J. Fluid Mech.* **278**, 267–287 (1994).
- Zia, I., R. G. Cox, and S. G. Mason, "Ordered aggregates of particles in shear flow," *Proc. R. Soc. London, Ser. A* **300**, 421–441 (1967).